Novel Pyrochlorelike Crystal with a Photonic Band Gap Self-Assembled Using Colloids with a Simple Interaction Potential

Harini Pattabhiraman,* Guido Avvisati, and Marjolein Dijkstra†
Soft Condensed Matter, Debye Institute for Nanomaterials Science, Department of Physics, Utrecht University, Princetonplein 5, 3584 CC Utrecht, Netherlands
(Received 11 May 2017; published 13 October 2017)

Using computer simulations, we investigate the phase behavior of a system of particles interacting with a remarkably simple repulsive square-shoulder pair potential and report the formation of a novel (and stable) pyrochlorelike crystal phase. The lattice structure of the pyrochlorelike phase formed in our simulations possesses two inherent length scales corresponding to the inter- and intratetrahedral neighbors. We show that it can be used to fabricate a photonic crystal which displays complete photonic band gaps in both the direct and inverted dielectric structures.

DOI: 10.1103/PhysRevLett.119.157401

Photonic crystals or photonic band gap (PBG) materials are periodic structures that prevent the propagation of light with specific wavelengths in all directions. Since their initial proposal in 1987 [1,2], there has been a huge interest in fabricating PBG materials with band gaps in the wavelengths pertaining to the visible and near-infrared region, because of their wide applicability [3,4]. For example, three-dimensional PBG materials possessing a band gap centered around 1.5 μm are interesting for applications not only in the telecommunication sector as lossless wave guides [5] and nonlinear optical switches [6] but also in (bio)sensing, biomedical engineering, and energy storage and security [7–10]. The current forerunners for these PBG materials are the dielectric diamond and pyrochlore structures created from precursor colloidal particles. They not only display a gap at a low refractive-index contrast ratio (around 2) and possess a large band gap width-to-frequency ratio but also exhibit a band gap at low-lying bands that are more stable against disorder [11]. However, the major obstacle in experimentally realizing these PBG materials is the fact that these structures are generally composed of an open (non-close-packed) arrangement of particles. This results in the lack of an inexpensive and reliable means of fabrication.

There has been a great effort to fabricate the diamond and the pyrochlore structures. One of the earlier methods to fabricate the diamond structure was the laborious process of nanorobotic manipulation of colloids [12]. In the case of the pyrochlore structure, a fabrication method involving an arduous layer-by-layer growth procedure was proposed [13]. A less laborious alternative to these is the directed self-assembly of the colloidal analogue of the $MgCu_2$ Laves phase from a binary colloidal dispersion [4,14,15]. One of the components of the Laves phase can then be selectively removed to obtain either the diamond or the pyrochlore lattice. In general, popular methods considered for the fabrication of open structures are the use of colloidal particles with selective patches [16–21] or self-assembly of colloids with complex interaction potentials [22–25]. However, these complicated potentials need to be heavily tuned, which makes their experimental realization difficult. The formation of near-visible PBG materials with either the diamond or the pyrochlore symmetry using colloidal particles of an appropriate size range from any of these routes has not been experimentally realized until now.

In this work, using computer simulations, we study the formation of photonic crystals in a system with a simple interaction potential that may be experimentally realized. This system emulates particles with a hard core surrounded by a squishy corona and has previously been realized in, for example, spherical dendrite micelles consisting of a rigid aromatic core with a deformable shell of alkyl chains [26] or block copolymer micelles consisting of a micellar core of hydrophobic polymer surrounded by a large shell of hydrophilic polymer blocks [27–31]. In this work, we consider this core-corona model to represent polymer-grafted colloidal nanoparticles [32]. We model this system using an interaction potential with a hard core of diameter σ_{HS} and a purely repulsive square shoulder of diameter δ. This radially symmetric hard-core square shoulder (HCSS) pair potential can be written as

$$V_{\mathrm{HCSS}}(r) = \begin{cases} \infty, & r \le \sigma_{HS}, \\ \epsilon, & \sigma_{HS} < r \le \delta, \\ 0, & r > \delta, \end{cases} \tag{1}$$

with r the interparticle center-of-mass distance and $\epsilon > 0$ the height of the square shoulder. The HCSS potential introduces two characteristic length scales in the system, namely, the hard-core diameter σ_{HS} and the square shoulder diameter δ. We define ϵ and σ_{HS}, respectively, as the units of energy and length.

So why do we chose this particular system? In other words, how does the HCSS system promote the formation

of open and non-close-packed structures like the pyrochlore? First, given the purely repulsive interactions between the particles in the HCSS system, one could expect the formation of crystal phases at low densities, i.e., open particle arrangements, rather than the gas-liquid condensation reported in systems with attractive interactions. Second, the phase behavior of this core-corona system is greatly influenced by δ. At $\delta \sim \sigma_{HS}$, the system behaves similar to a system of hard spheres, while for $\delta \gg \sigma_{HS}$, the hard core becomes effectively irrelevant at low temperatures. However, an interplay between the energetic and entropic contributions promotes the formation of phases with exotic structures at intermediate shoulder widths. For example, self-assembly of stripelike mesophases has been reported in a two-dimensional HCSS system at shoulder widths of 2.0 [32,33] and 2.5 [34,35] times the hard-disk diameter σ, and clusters of various sizes have been reported at larger shoulder widths, i.e., $3.0\sigma \leq \delta \leq 10.0\sigma$ [36]. Similar clustering behavior has also been reported in a three-dimensional HCSS system at $\delta = 4.5\sigma_{HS}$ and $10\sigma_{HS}$ [37,38].

To begin with, we performed a preliminary study on the phase behavior of the HCSS system with similar sizes of the hard core and the surrounding shoulder in order to identify the lower limit of the formation of clusters in the HCSS system. We used a range of shoulder widths $1.90\sigma_{HS} \leq \delta \leq 2.10\sigma_{HS}$. We found that the system exhibited the formation of tetrahedral clusters at $\delta \geq 1.95\sigma_{HS}$. We, then, proceeded to a detailed study of the phase behavior of the HCSS system at a constant shoulder width of $\delta = 2.10\sigma_{HS}$ and studied the formation of a pyrochlore lattice, which can be considered to be composed of tetrahedral clusters [14,39]. To this end, we perform Monte Carlo simulations using a system of N particles in a cubic box of volume V with periodic boundary conditions in the canonical (NVT) and isothermal-isobaric (NPT) ensembles. We define various reduced (dimensionless) physical quantities to describe the system, namely, temperature $T^* = k_B T/\epsilon$, pressure $P^* = \beta P \sigma_{HS}^3$, and density $\rho^* = N\sigma_{HS}^3/V$, where $\beta = 1/k_B T$ is the inverse temperature with k_B the Boltzmann constant. Depending on the lattice structure, a system size N between 432 and 512 particles is used for the NPT studies. Subsequently, we map out the phase diagram by calculating the Helmholtz free energy of different phases and employing common tangent constructions. We employ the Frenkel-Ladd method [40,41] to calculate the free energy of various crystal phases at the high-density regimes. For the free-energy calculation of other low-density phases and the isotropic fluid, we employ the Schilling-Schmid method [42,43].

The calculated phase diagram in the temperature-density plane is shown in Fig. 1. The first observation we make is the rich phase behavior displayed by the system. We identify and mark the following phases: an isotropic fluid (FL), a body-centered cubic (bcc), a face-centered cubic (fcc) phase at three distinct density ranges, namely, a high- (hfcc), a medium- (mfcc), and a low-density (lfcc) face-centered cubic, a pyrochlorelike phase (PYR), and a hexagonal columnar phase (col). The col phase is a three-dimensional manifestation of the previously mentioned two-dimensional stripe phase. Sample configurations showing the structure of the col phase are given in Supplemental Material [44]. The driving force for the formation of fcc phases in these three different density regimes is the presence of the two length scales in the system. The lfcc forms when the nearest-neighbor distance approximately corresponds to the diameter of the corona, and the hfcc forms when the nearest neighbors are approximately at a distance that equals the hard-core diameter. In the mfcc phase, the second-nearest neighbors are at a distance equal to the square shoulder diameter δ. At temperatures higher than those reported here, we expect the system to display a behavior similar to that of the hard-sphere system with FL at low densities and hfcc at high densities and a two-phase coexistence region in between (not shown here). The region of interest in this phase diagram is the reentrant phase behavior of the fluid which encompasses various low-density open structures like lfcc, col, and PYR.

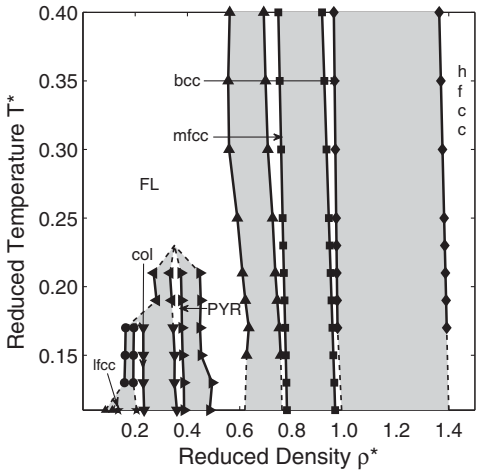

FIG. 1. Phase diagram in the temperature-density representation obtained for the HCSS system with shoulder width $\delta = 2.10\sigma_{HS}$. The reduced quantities are defined as $T^* = k_B T/\epsilon$ and $\rho^* = N\sigma_{HS}^3/V$. The phases shown are FL, bcc, hfcc, mfcc, lfcc, PYR, and col. The gray regions denote the two-phase coexistence regions.

Of these low-density structures, we focus exclusively on the PYR phase here, which can be used as a precursor to a dielectric photonic crystal. The ideal pyrochlore lattice (iPYR) is composed of tetrahedral clusters with their centers positioned in the tetrahedral voids of a diamond lattice [39]. At its maximum packing density ($\rho^* = 0.71$), each particle has six equidistant nearest neighbors, i.e., the other three particles in the same tetrahedron (intratetrahedral) and the nearest particle from the three neighboring

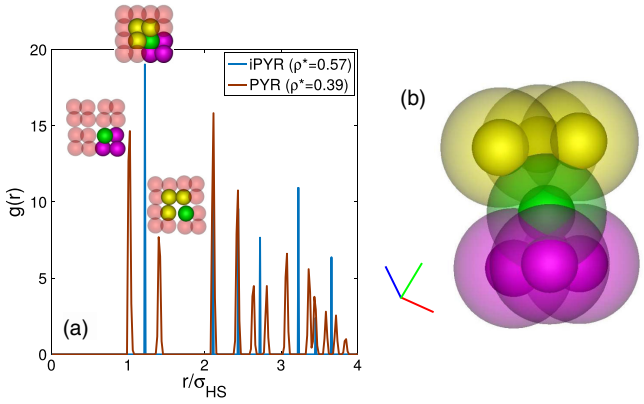

FIG. 2. (a) Radial distribution function $g(r)$ for the iPYR and the PYR obtained in our simulations at densities where the positions of the peaks at $r = 2.10\sigma_{HS}$ match. The intra- (purple) and intertetrahedral (yellow) neighbors of a particle (green) corresponding to a certain peak are highlighted in the sample configurations given in the insets. (b) A sample configuration of PYR showing the intra- (purple) and intertetrahedral (yellow) neighbors of a particle (green) along with their coronas.

tetrahedra (intertetrahedral). However, we find that not all the six neighbors of a particle are equidistant in our pyrochlorelike structure, which is formed by expanding a bcc lattice to lower pressure at a constant temperature. In fact, the distance between inter- and intratetrahedral neighbors is different, which results in a substantially lower maximum density for this structure ($\rho^* = 0.39$).

We present a comparison between the PYR and iPYR structures in Fig. 2 by comparing the radial distribution functions (RDFs) and particle neighbors. In Fig. 2(a), the RDF of the PYR phase is calculated at a density that corresponds to the close packing of the intratetrahedral neighbors ($\rho^* = 0.39$), and the density of the iPYR phase ($\rho^* = 0.57$) is chosen such that it matches the peak positions corresponding to the square shoulder at $r = 2.10\sigma_{HS}$. Here, we can clearly note that the first (single) peak of iPYR is split into two in the case of PYR. These two peaks correspond to the inter- and intratetrahedral neighbors as shown in the inset. Furthermore, we take a closer look at the structure of PYR by drawing the surrounding coronas of the particles in Fig. 2(b). Here, for a certain particle (in green), we can see that the intertetrahedral neighbors (in yellow) are positioned such that their coronas do not overlap with those of the intratetrahedral neighbors (in purple). This hints that this structure is stabilized by minimization of the overlap of the repulsive corona with the neighboring particles, i.e., an energetic stabilization of this structure. This is, in fact, similar to the formation of stripe or honeycomb phases in two-dimensional HCSS systems [49]. We have not found any previous reports of an energetically stabilized pyrochlore phase in systems of isotropic particles. However, there has been one theoretical report of entropic stabilization of the iPYR structure in a system of triblock Janus particles [21]. The resulting phase diagram consists of a mixture of iPYR and hexagonal tetrastack lattices [21].

Having characterized the PYR structure, we next investigate whether or not it displays a complete photonic band gap and how it is affected by the peak splitting in the RDF. We also calculate the band structure of the iPYR for comparison. Photonic crystals can be fabricated from self-assembled colloidal crystals by a process involving infiltration with a high-dielectric constant material and template removal [10]. For the purpose of illustration, we chose the high-dielectric constant material to be silicon and the low-dielectric constant material to be air. The dielectric constant of silicon is taken to be 12, and that of air is unity. For our calculations, we consider both the direct structure consisting of silicon spheres in air and the inverse structure made of air spheres in silicon. The effect of the band gap width as a function of dielectric contrast is given in Supplemental Material [44]. The photonic properties of the dielectric pyrochlore structure are numerically evaluated using the freely available "MIT Photonic-Bands" software package [50]. This software computes fully vectorial eigenmodes of Maxwell's equations with periodic boundary conditions by a preconditioned conjugate-gradient minimization of the block Rayleigh quotient in a plane wave basis [50]. We discretize the unit cell using a grid consisting of 32 grid points in each direction. The photonic properties of the two pyrochlore structures are compared in terms of two quantities: (i) the position of the band gap in terms of the reduced frequency $\omega^* = \omega a/2\pi c$, where ω is the frequency of the electromagnetic field, a is the length of a side of the unit cell, and c is the speed of light in vacuum, and (ii) the relative gap width $\Delta\omega/\omega_m$, where $\Delta\omega$ is the gap width and ω_m is the midgap frequency. It is well established that the iPYR structure possesses a complete photonic band gap [4,13,39,51]. The direct dielectric structure of iPYR consisting of silicon spheres in air has a maximum gap width $\Delta\omega/\omega_m = 13\%$ between bands 2 and 3 for a dielectric density of $\rho^* = 0.88$, while the inverse structure of air spheres in silicon has a maximum gap width of $\Delta\omega/\omega_m = 26\%$ at an air density $\rho^* = 2.52$. Given that the maximum density of the iPYR is $\rho^* = 0.71$, the particles overlap with the neighboring particles in both these cases. Such a structure with overlapping particles can be fabricated either by sintering and subsequent growth of the particles [3,52] or by growing a polymer layer around the particles [53].

A comparison between the photonic properties of the PYR and iPYR in terms of the relative band gap width and the corresponding band gap map is given in Fig. 3. The band gap map involves plotting the locations of the extremities of the photonic band gap in the band structure as a function of a geometrical parameter, i.e., the hard-core diameter σ_{HS}. For convenience, we represent this in terms of the density of the structure ρ^*. In Figs. 3(a) and 3(b), we investigate the direct structures consisting of silicon spheres

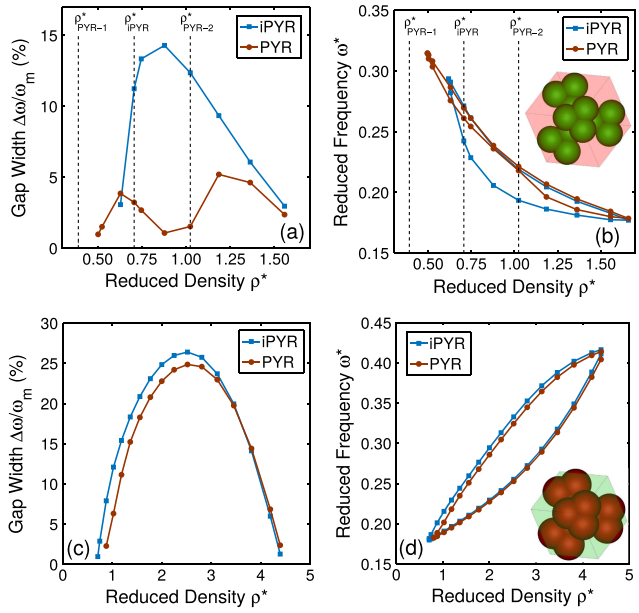

FIG. 3. Comparison of the photonic properties of pyrochlore structures, namely, the iPYR and the PYR obtained in our simulations: (a),(c) relative gap width $\Delta\omega/\omega_m$ as a function of (reduced) density $\rho^* = N\sigma_{HS}^3/V$ and (b),(d) band gap map calculated for (a),(b) a direct structure of silicon spheres in air and (c),(d) an inverse structure of air spheres in silicon. In (a),(b), the densities where the particles start to overlap in iPYR (ρ^*_{iPYR}) and where the particles in a tetrahedron $(\rho^*_{\text{PYR-1}})$ and between neighboring tetrahedra $(\rho^*_{\text{PYR-2}})$ start to overlap in a PYR lattice are individually marked. The reduced frequency is written as $\omega^* = \omega a/2\pi c$. A representation of the configuration of PYR pertaining to the density at which the maximum band is obtained is given in (b) for the direct ($\rho^* = 1.18$) structure and in (d) for the inverse ($\rho^* = 2.52$) structure. Here, the green and red colors, respectively, denote silicon and air.

in air, while in Figs. 3(c) and 3(d), we investigate the inverse structure consisting of air spheres in silicon. Please note that the density given in the direct structures represents that of silicon spheres and that in the inverse structures represents that of air spheres. The size of the error bars in these plots are of the size of the markers.

First, let us look at the direct structures. In Fig. 3(a), we plot the band gap width as a function of (reduced) density ρ^*, and in Fig. 3(b), we show the band gap map. In addition, we draw vertical dashed lines to denote the maximum density of the iPYR ρ^*_{iPYR} and the two relevant densities in PYR, i.e., $\rho^*_{\text{PYR-1}}$ where the intratetrahedral neighbors are in contact and $\rho^*_{\text{PYR-2}}$ where the intertetrahedral neighbors are in contact and the intratetrahedral neighbors overlap with each other. From these figures, we see that both the PYR and iPYR structures possess a complete band gap. However, the band gap width obtained in iPYR is much larger than in our PYR structure. Given that all parameters used in these two structures is the same, it is tempting to speculate that the difference in the photonic properties is due to the observed peak splitting in PYR. We note that the band gap width in the case of iPYR reaches a maximum at a density slightly larger than ρ^*_{iPYR}, while in the case of PYR two maxima are found at densities slightly higher than both the relevant densities $\rho^*_{\text{PYR-1}}$ and $\rho^*_{\text{PYR-2}}$. This can be seen as a manifestation of the peak splitting as described in Fig. 2(a), which makes both these length scales relevant in the PYR structure. Even though the PYR does not possess a band gap at its maximum density $\rho^*_{\text{PYR-1}}$, it does at higher densities. This could be obtained by sintering the silicon particles as shown in the inset in Fig. 3(b). We note that sintering, and further growth of the particles, when performed subsequent to the self-assembly, does not affect the structure in the case where it is close packed [52].

On the other hand, we do not see a huge difference in the photonic behavior of the inverse structures of PYR and iPYR as shown in Figs. 3(c) and 3(d). In the case of these inverse photonic crystals, the primary structure is a connected dielectric network, and a photonic band gap is generated when this network is interrupted by air particles. One could speculate that the peak splitting does not have a huge influence in modifying the properties of an already connected dielectric network, thereby leading to similar photonic properties of the two inverse structures.

In summary, our simulations demonstrate the self-assembly and stability of a pyrochlorelike lattice using a simple yet experimentally attainable interaction potential. This structure can be used as a precursor to a dielectric photonic crystal possessing a complete photonic band gap. Furthermore, the pyrochlorelike structure formed in our simulations is also unique in its structure; i.e., its inter- and intratetrahedral neighbors are not equidistant. We find that the formation of this phase is robust across a range of shoulder widths ($1.95\sigma_{HS} \leq \delta \leq 2.25\sigma_{HS}$) and system sizes (up to 10^4 particles) as given in Supplemental Material [44]. We point out here that the effective potential of experimental realizations of core-corona particles is likely not a square-shoulder potential but more a soft repulsive potential. We have previously found that the phase behavior in core-corona systems is rather robust against different shapes of the interaction potential as long as the two length scales are maintained [54]. Furthermore, our comparison of the photonic properties of this novel pyrochlorelike structure with that of the ideal pyrochlore lattice shows that (i) the inverse dielectric structures exhibit similar photonic properties and (ii) the peak splitting has a greater effect on the photonic properties of the direct dielectric structure than the inverse one.

This work is part of the Industrial Partnership Program "Computational Sciences for Energy Research (CSER)" (12CSER004) and of the FOM projectruimte, both of the Foundation for Fundamental Research on Matter (FOM), which is part of the Netherlands Organisation for Scientific Research (NWO). The CSER program is cofinanced by Shell Global Solutions International B. V. We thank Simone Dussi and Laura Filion for critical reading of

the manuscript. H. P. constructed the phase diagram and performed the photonic properties calculations. H. P. and G. A. jointly performed the cluster identification and radial distribution function calculations. M. D. coordinated the study and helped write the manuscript.

*h.pattabhiraman@uu.nl
†m.dijkstra@uu.nl

[1] S. John, Phys. Rev. Lett. **58**, 2486 (1987).
[2] E. Yablonovitch, Phys. Rev. Lett. **58**, 2059 (1987).
[3] K. Busch and S. John, Phys. Rev. E **58**, 3896 (1998).
[4] A.-P. Hynninen, J. H. J. Thijssen, E. C. M. Vermolen, M. Dijkstra, and A. van Blaaderen, Nat. Mater. **6**, 202 (2007).
[5] S. Noda, K. Tomoda, and N. Yamamoto, Science **289**, 604 (2000).
[6] H. Han, S. Vijayalakshmi, A. Lan, Z. Iqbal, H. Grebel, E. Lalanne, and A. M. Johnson, Appl. Phys. Lett. **82**, 1458 (2003).
[7] J. Ge and Y. Yin, Angew. Chem., Int. Ed. **50**, 1492 (2011).
[8] J. Xu and Z. Guo, J. Colloid Interface Sci. **406**, 1 (2013).
[9] G. von Freymann, V. Kitaev, B. V. Lotsch, and G. A. Ozin, Chem. Soc. Rev. **42**, 2528 (2013).
[10] A. Stein, B. E. Wilson, and S. G. Rudisill, Chem. Soc. Rev. **42**, 2763 (2013).
[11] Z.-Y. Li and Z.-Q. Zhang, Phys. Rev. B **62**, 1516 (2000).
[12] F. García-Santamaría, H. T. Miyazaki, A. Urquía, M. Ibisate, M. Belmonte, N. Shinya, F. Meseguer, and C. López, Adv. Mater. **14**, 1144 (2002).
[13] A. J. Garcia-Adeva, New J. Phys. **8**, 86 (2006).
[14] G. Avvisati, T. Dasgupta, and M. Dijkstra, ACS Nano. **11**, 7702, (2017).
[15] É. Ducrot, M. He, G.-R. Yi, and D. J. Pine, Nat. Mater. **16**, 652, (2017).
[16] Z. Zhang, A. S. Keys, T. Chen, and S. C. Glotzer, Langmuir **21**, 409 (2005).
[17] E. G. Noya, C. Vega, J. P. K. Doye, and A. A. Louis, J. Chem. Phys. **132**, 234511 (2010).
[18] F. Romano, E. Sanz, and F. Sciortino, J. Chem. Phys. **132**, 184501 (2010).
[19] X. Mao, Phys. Rev. E **87**, 1 (2013).
[20] X. Mao, Q. Chen, and S. Granick, Nat. Mater. **12**, 217 (2013).
[21] D. Z. Rocklin and X. Mao, Soft Matter **10**, 7569 (2014).
[22] M. Dzugutov, Phys. Rev. A **46**, R2984 (1992).
[23] M. C. Rechtsman, F. H. Stillinger, and S. Torquato, Phys. Rev. E **74**, 021404 (2006).
[24] M. Engel, P. F. Damasceno, C. L. Phillips, and S. C. Glotzer, Nat. Mater. **14**, 109 (2015).
[25] P. F. Damasceno, S. C. Glotzer, and M. Engel, J. Phys. Condens. Matter **29**, 234005 (2017).
[26] X. Zeng, G. Ungar, Y. Liu, V. Percec, A. E. Dulcey, and J. K. Hobbs, Nature (London) **428**, 157 (2004).
[27] A. Takano, W. Kawashima, A. Noro, Y. Isono, N. Tanaka, T. Dotera, and Y. Matsushita, J. Polym. Sci., Part B: Polym. Phys. **43**, 2427 (2005).
[28] T. Dotera and T. Gemma, Philos. Mag. **86**, 1085 (2006).
[29] K. Hayashida, T. Dotera, A. Takano, and Y. Matsushita, Phys. Rev. Lett. **98**, 195502 (2007).
[30] S. Lee, M. J. Bluemle, and F. S. Bates, Science **330**, 349 (2010).
[31] S. Fischer and A. Exner, Proc. Natl. Acad. Sci. U.S.A. **108**, 1 (2011).
[32] Y. Norizoe and T. Kawakatsu, Europhys. Lett. **72**, 583 (2005).
[33] Y. Norizoe and T. Kawakatsu, J. Chem. Phys. **137**, 024904 (2012).
[34] G. Malescio and G. Pellicane, Nat. Mater. **2**, 97 (2003).
[35] G. Malescio and G. Pellicane, Phys. Rev. E **70**, 021202 (2004).
[36] J. Fornleitner and G. Kahl, J. Phys. Condens. Matter **22**, 104118 (2010).
[37] G. J. Pauschenwein and G. Kahl, Soft Matter **4**, 1396 (2008).
[38] G. J. Pauschenwein and G. Kahl, J. Chem. Phys. **129**, 174107 (2008).
[39] T. T. Ngo, C. M. Liddell, M. Ghebrebrhan, and J. D. Joannopoulos, Appl. Phys. Lett. **88**, 241920 (2006).
[40] D. Frenkel and B. Smit, *Understanding Molecular Simulation: From Algorithm to Applications* (Academic Press Inc., New York, 1996), ISBN 0-12-267351-4.
[41] C. Vega and E. Sanz, J. Phys. Condens. Matter **20**, 153101 (2008).
[42] T. Schilling and F. Schmid, J. Chem. Phys. **131**, 231102 (2009).
[43] F. Schmid and T. Schilling, Phys. Procedia **4**, 131 (2010).
[44] See Supplemental Material at http://link.aps.org/supplemental/10.1103/PhysRevLett.119.157401 for more information, which includes Refs. [45–48].
[45] X. Zeng, F. Liu, A. G. Fowler, G. Ungar, L. Cseh, G. H. Mehl, and J. E. Macdonald, Adv. Mater. **21**, 1746 (2009).
[46] M. M. Wojcik, M. Gora, J. Mieczkowski, J. Romiszewski, E. Gorecka, and D. Pociecha, Soft Matter **7**, 10561 (2011).
[47] B. A. Lindquist, S. Dutta, R. B. Jadrich, D. J. Milliron, and T. M. Truskett, Soft Matter **13**, 1335 (2017).
[48] K. P. Velikov, A. Moroz, and A. van Blaaderen, Appl. Phys. Lett. **80**, 49 (2002).
[49] H. Pattabhiraman and M. Dijkstra, Soft Matter **13**, 4418 (2017).
[50] S. Johnson and J. Joannopoulos, Opt. Express **8**, 173 (2001).
[51] A. J. Garcia-Adeva, Phys. Rev. B **73**, 073107 (2006).
[52] H. Míguez, F. Meseguer, C. López, Á. Blanco, J. S. Moya, J. Requena, A. Mifsud, and V. Fornés, Adv. Mater. **10**, 480 (1998).
[53] A. Stein, F. Li, and N. R. Denny, Chem. Mater. **20**, 649 (2008).
[54] H. Pattabhiraman and M. Dijkstra, J. Phys. Condens. Matter **29**, 094003 (2017).